Available online at www.CivileJournal.org

# Civil Engineering Journal

(E-ISSN: 2476-3055; ISSN: 2676-6957)

Vol. 12, No. 06, June, 2026

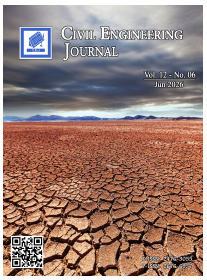

# Artificial Neural Network Prediction of Sediment Reduction Ratio in Open Channel Flows

Ali Sadiq Abbas [1*]

[1] *Department of Civil Engineering, University of Technology, Baghdad 10071, Iraq.*

Received 18 March 2026; Revised 15 May 2026; Accepted 17 May 2026; Published 01 June 2026

**Abstract**

The ecological equilibrium and structural integrity of open waterways are significantly influenced by the effective management of sediment within hydraulic systems. Although conventional experimental testing methods are precise, they are frequently time-consuming and expensive. This study describes a unique computational technique that uses Artificial Neural Networks (ANNs) to anticipate the Sediment Reduction Ratio (SRR) in open channel flows, offering an alternative to significant physical experiments. The ANN model was trained on a constrained dataset that was obtained from studies that evaluated sediment flow under varied weir heights and channel bed inclinations. The model's performance was rigorously assessed using a variety of metrics, such as the coefficient of determination ($R^2$), coefficient of variation of the root means square error (CVRMSE), mean squared error (MSE), root mean squared error (RMSE), mean absolute error (MAE), and mean absolute percentage error (MAPE). The model demonstrated exceptional performance, with an MSE of 0.007%, RMSE of 0.87%, MAE of 0.76%, MAPE of 0.84%, CVRMSE of 0.93%, and a $R^2$ of 0.99. These results indicate that the ANN is capable of accurately and consistently predicting SRR, thereby offering hydraulic engineers a potent instrument for simulating sediment behavior. This study emphasizes the revolutionary potential of machine learning in environmental engineering, allowing for the creation of more cost-effective and adaptable sediment control systems.

*Keywords:* Ratio of Sediment Reduction; Open Channels; Machine Learning; Artificial Neural Networks.

## 1. Introduction

Sediment movement and deposition in open channels pose significant challenges to the health of aquatic habitats, water quality, and hydraulic infrastructure [1-4]. A range of interacting elements impact sediment movement dynamics, including hydraulic structures such as weirs, bed slope, channel geometry, sediment particle size distribution, and flow velocity [5-8]. Physical tests and empirical rating curves, despite their correctness, are often used in traditional sediment management techniques; nevertheless, replicating them under varied hydraulic circumstances is time-consuming, labor-intensive, and expensive [9, 10].

In response to these limits, formal computational modeling has emerged as a viable option. For example, Allawi et al. [11] compared random forest, MLP, SVR, and LSTM models to anticipate scattered sediment load. They determined that the LSTM provided the highest level of accuracy. To model sewer sediment movement, Gul et al. [12] used ensemble and hybrid algorithms optimized using the Runge-Kutta optimizer. For sediment transport prediction, Ebtehaj et al. [13] enhanced ANN using the imperialist competitive algorithm (ICA), particle swarm optimization (PSO), and genetic algorithm (GA). The ICA-ANN model has the lowest amount of uncertainty. Table 1 provides a concise review of the most important research.

* Corresponding author: 40005@uotechnology.edu.iq

https://doi.org/10.28991/CEJ-2026-012-06-018

Nevertheless, despite these advancements, there are still a number of critical research deficits. Initially, the vast majority of current machine learning models for sediment prediction were developed and verified using extensive, high-frequency datasets [11, 14]. The effectiveness of these models in data-scarce conditions, which are common in developing regions or rapidly changing environments, is primarily unexplored. Secondly, hybrid and ensemble models (e.g., ANFIS, GA-ANN, PSO-ANN) offer high accuracy; however, they require meticulous parameter tuning and introduce substantial computational complexity [13, 15]. Despite their potential for useful, low-cost implementation, simplified ANN architectures with limited calibration have received relatively little attention. Third, the Sediment Reduction Ratio (SRR)—a critical metric for assessing the efficacy of sediment control structures like weirs—has not been systematically modeled using machine learning, whereas existing research has primarily concentrated on predicting suspended sediment load or total sediment transport [11, 13, 16]. Fourth, the experimental dataset provided by Omran et al. [17] has never been employed to train or validate an ANN model for SRR prediction. In an open channel, this dataset systematically varies weir heights (0.5B, B, 1.5B), bed gradients (0.015, 0.0225, 0.03), and flow velocities (100–300 L/min).

For their assessment, Yaseen et al. [18] looked on the developments in seepage analysis AI applications from 2015 to 2024. The most cutting-edge AI models were shown in the study over a range of geological settings. Regression, ensemble, evolutionary, deep learning, classical, hybrid, and AI models were all used for seepage modeling, as the review showed. Managing non-linear seepage occurrences was a breeze using the hybrid models. When it came to time-series forecasting, deep learning models performed well, but kernel and dimensionality reduction models significantly reduced computing demands. A number of issues with the offered literature were highlighted by the review. These included problems with data availability, model interpretation, and generalizability.

Tomar et al. [19] used a new Deep Neural Network (DNN) model tailored for sediment transport in river basins to enhance hydropower projects. The effectiveness of river systems' silt removal processes was examined using this model. By testing the effectiveness of sediment removal during long run periods (0-180 h) at flow rates ranging from 250 to 500 cumec, this study hopes to assess the dynamics of sedimentation under various discharge circumstances. The DNN model captures the intricate link between sediment transport patterns and discharge parameters by using crucial inputs such as river flow and sediment concentration measurements to anticipate the efficacy of sediment removal. A discharge rate of 374.40 cumec and an ideal sediment content of 2497.61 ppm were achieved by optimizing the operating parameters using Differential Evolution Optimization. At the same time that it reduces turbine attrition caused by silt deposition, it ensures optimum functioning. The model also found the ideal conditions for the diversion tunnel, which were kept at 130 cumec and 2714.87 ppm for 97.12 hours to ensure a balanced sediment flow.

Table 1 provides a synopsis of the present study that outlines how the research is using machine learning techniques to improve hydraulic system sediment-related process prediction and management. Integrating state-of-the-art computational techniques, such as evolutionary algorithms, ANNs, and other composite models, into these investigations shows a considerable improvement over previous systems in terms of the accuracy of material movement prediction and management. Specifically, ensemble and composite models enhance the accuracy and dependability of predictions. It is clear that using machine learning may make sediment management tactics more adaptable and long-lasting.

**Table 1. A summary of significant research on sediment-corresponding predictions and applications**

| Ref. | Machine Learning Approach | Methodology | Key Findings |
|---|---|---|---|
| Allawi et al. [11] | LSTM, MLP, SVR, RF | Prediction of suspended sediment load | High correlation between predicted and actual SSL; LSTM model achieved the highest accuracy. |
| Gul et al. [12] | ELM, MLPNN, M5PMT; RUN, GA, PSO | Optimization and ensemble hybrid algorithms | RUN-based hybrid models outperformed others; MLPNN-M5PMT had slightly better performance than MLPNN-RUN. |
| Khosravi et al. [15] | Hybrid data mining algorithms | Prediction of stable gravel-bed river hydraulic geometry | Hybrid models outperformed standalone models; Vote-Kstar and ASC-Kstar provided very good performance. |
| Safari et al. [16] | GEP, ELM, GS-GMDH, FCM-ANFIS | Modeling of sediment transport | GS-GMDH showed slightly better performance compared to other models; comprehensive model comparisons made. |
| Barman et al. [14] | SWAT-ANN | Analysis of climate change impacts on sediment yield | Hybrid model significantly improved accuracy over standalone SWAT model; detailed impact analysis provided. |
| Ebtehaj et al. [13] | ANN with PSO, ICA, GA | Prediction of sediment transport without sedimentation | ICA-ANN model provided the lowest prediction uncertainty; outperformed other hybrid models. |
| Yaseen et al. [18] | ANN with GIS | Forecasting urban expansion effects on sediment yield | Demonstrated increased sediment yield and runoff due to urban expansion; used ANN and GIS integration |

Despite the significant progress in machine learning for sediment behavior forecasting that the reviewed literature highlights, there are still numerous research gaps and limitations. Initially, regardless the exploration of a variety of machine learning models, there is still a dearth of research that concentrates on optimizing these models for sediment prediction with minimal experimental data. The vast majority of studies depend on extensive datasets, which may not be feasible in all geo-graphical contexts, in particular in under-resourced or swiftly changing

environments. In addition, the lack of consensus regarding the metrics that the majority accurately reflect the performance of models in the removal of sediment or reduction applications is indicated by the diversity of evaluation metrics utilized across studies, which may confound comparative analyses. The goal of this paper is to address these voids by introducing a number of novelties in the application of ANNs to sediment management. These changes include:

- The significant departure from conventional heavy experimental configurations is shown by the optimization of performance with limited input data through the customization of the architecture and calibration of the ANN.
- To ensure the forecasting capabilities' exhaustive validation and to conduct a multi-dimensional analysis of the ANN's efficacy, a diverse selection of performance parameters is employed.
- Showing how machine learning may replace time-consuming and labour-intensive experimental procedures, leading to more accurate and scalable sediment predictions.

The following novelties are discussed in the present analysis to resolve these gaps:

- Building a simple two-hidden-layer ANN model to predict SRR using a small experimental dataset (27 situations) to show that much data isn't always necessary for accurate results.
- To guarantee strong validation, the model's performance was rigorously evaluated across three distinct tests and three different weir heights using seven complementing metrics: MSE, RMSE, MAE, MAPE, CVRMSE, and $R^2$.
- First application of machine learning to the SRR-specific dataset of Omran et al. [17], providing a baseline for future studies.
- Demonstration that a computational alternative can achieve accuracy comparable to physical experiments ($R^2$ = 0.99, MSE = 0.007%), thereby reducing reliance on costly and time-intensive laboratory testing.

Using a small experimental dataset, this research aims to develop, train, and validate an artificial neural network (ANN) model for the prediction of the Sediment Reduction Ratio (SRR) in hydraulic open channels with different weir heights, bed gradients, and flow rates.

The following is the structure of the paper's remaining section: The experimental setup, sediment properties, and methods of data collecting are detailed in Section 2. In Section 3, you can find comprehensive explanations of the ANN's design, training method, and performance indicators. In Section 4, we see the model's predictions and talk about what they mean. Section 5 presents the findings and recommendations for further study.

## 2. Materials and Methods

### 2.1. Sediment Source and Collection

The experimental silt came from a spot upstream of the experimental facility, in the bed of the Euphrates River (coordinates: [to be supplied by author]). After being mixed, air-dried, and filtered through a 2-mm screen, the sediment was used to remove organic debris and big particles. After that, the sediment was stored in airtight containers to keep its moisture content (about 2% to 3% by mass) constant throughout the experiment.

### 2.2. Particle Size Distribution

Dry sieving was used for particle size analysis in compliance with ASTM D6913 [20]. Utilizing a mechanical agitator, a set of standard sieves with aperture widths ranging from 2.00 mm to 0.125 mm and 0.063 mm was positioned for fifteen minutes. To get the total passing percentage, we measured the mass that remained on each sieve.

With d10 = 0.18 mm and d60 = 0.42 mm, the median particle diameter (d50) is 0.32 mm. The uniformity coefficient (Cu = d60/d10) is 2.33, whereas the coefficient of curvature ($Cc = d30^2/(d10 \times d60)$) is 0.83. Based on the Unified Soil Classification System (USCS), these results suggest that the sediment is SP, or poorly graded sand. The modest size range (0.18-0.42 mm for 80% of the material) suggests limited gradation and makes it simpler to examine sediment transport dynamics by decreasing the influence of differential settling across particle sizes.

### 2.3. Particle Density and Shape

The sediment particles' specific gravity (Gs) was determined according with ASTM D854 [21] using a water pycnometer. Gs = 2.65, which is typical for sediments dominated by quartz, was determined by the average of three measurements. The sediment bed's dried bulk density was determined to be 1.62 g/cm³, which is equivalent to a porosity of approximately 0.39.

Microscopic imaging was employed to evaluate the morphology of 200 granules that were arbitrarily selected (ASTM F1877) [22]. The average shape factor (S.F.) was 0.71, with a standard deviation of 0.09. This is defined as the ratio of the particle's shortest to longest orthogonal axis. This value suggests that the granules are well-rounded to sub-rounded, which is a characteristic of fluvial sediments that have been transported over significant distances. The sedimentation diameter, which is equivalent to the diameter of a sphere with an equivalent settling velocity, was determined to be approximately 0.7 × d50 = 0.22 mm, in accordance with the shape factor correction.

## 2.4. Experimental Setup

The investigations were conducted in the hydraulics laboratory of the Department of Civil Engineering, University of Technology, Baghdad, in a recirculating open-channel flume. Figure 1 shows a schematic diagram of the experimental apparatus.

The entire length of the flume is 10 meters, and its rectangular cross-section is 0.20 meters wide and 0.50 meters high. The sediment movement may be visually monitored via the use of tempered glass that encases the side walls. Stainless steel channel bed can tolerate three distinct longitudinal slopes: S1 = 0.015, S2 = 0.0225, and S3 = 0.03. A hydraulic lift mechanism is used to modify the slope at the downstream end. A constant-head reservoir connected to the source of the Euphrates River provides access to water. A calibrated rotameter and gate valve regulate three separate flow rates: 100 L/min, 200 L/min, and 300 L/min.

A 6-mm-thick acrylic plate is used to build a sharp-crested weir that is positioned five meters from the entrance and perpendicular to the direction of flow. H1 = 0.5B = 0.10 m, H2 = B = 0.20 m, and H3 = 1.5B = 0.30 m are three interchangeable weirs of different heights. B = 0.20 m is the canal width. The 2 mm thick weir crest has a 90° downstream chamfer, which helps to reduce flow separation. For sediment sampling, two separate locations are utilized: The first point, A, is located two meters upstream of the weir, while the second, B, is three meters downstream. Collecting water-sediment samples at mid-depth is done using 500 mL containers. For gravimetric determinations of sediment concentrations, the following steps are taken: filtration, dehydrating at 105°C for 24 hours, and weighing. For the sake of reproducibility, we run each experimental condition three times.

The flume is 10 meters long overall, with a rectangular cross-section of 0.20 meters in width and 0.50 meters in height. Three different slopes may be set for the channel bed: 0.015, 0.0225, and 0.03. At regulated flow rates of 100, 200, and 300 L/min, water is added from an upstream input. Five meters from the inlet lies a sharp-crested weir. H1 = 0.5B = 0.10 m, H2 = B = 0.20 m, and H3 = 1.5B = 0.30 m are the three interchangeable weir heights used. B = 0.20 m is the canal width. Two sample stations, Point B (downstream, 3 m after the weir) and Point A (upstream, 2 m before the weir), are used to measure the sediment content. A downstream outlet is used to release water. All dimensions are represented by double-headed symbols. A large horizontal arrow indicates the direction of flow.


**Figure 1. Hydraulic channel experimental workbench: (a) overall view; (b) close-up visualization [19]**

## 2.5. Measurement Techniques and Data Collection

### 2.5.1. Flow Rate Control and Measurement

The supply line was equipped with a calibrated rotameter (variable area flow meter) to monitor the flow rate, which was controlled by a gate valve. With an accuracy of ±2% of full scale, the rotameter can measure between 0 and 400 L/min. Every year, the volumetric technique was used for calibration, which included collecting water in a vessel with a specified volume over a predetermined period of time. Three distinct flow rates—100, 200, and 300 L/min—were used in the studies. After two minutes of continuous flow, the actual flow rate was recorded after the gate valve was adjusted for each target flow rate until the rotameter reading stabilized.

### 2.5.2. Bed Slope Adjustment and Measurement

The slope of the channel bed at the downstream end was changed using a hydraulic lift system. The slope was measured using a digital inclinometer (precision ±0.0005) directly on the channel bed at three longitudinal places (up-stream, mid-length, down-stream). The bed slope for this experimental arrangement was obtained by averaging the three measurements. Three gradients were evaluated: S1 = 0.015, S2 = 0.0225, and S3 = 0.030. The slope was verified prior to each experimental trial.

### 2.5.3. Weir Height Measurement

Three sharp-crested weirs were fabricated from 6-mm-thick acrylic sheet with heights of H1 = 0.10 m (0.5B), H2 = 0.20 m (B), and H3 = 0.30 m (1.5B), where B = 0.20 m is the channel width. The mean value was recorded after the actual height of every weir was measured at three locations along with the crest (left, center, right) utilizing a digital vernier calliper (accuracy ±0.01 mm). The weir was installed at a distance of 5 m from the inlet, perpendicular to the flow direction. In order to prevent underflow or lateral leakage, sealing membranes were implemented.

### 2.5.4. Sediment Sampling and Concentration Determination

The sediment content was determined at two sample points, Point A located 2 meters before to the weir and Point B located 3 meters downstream of the weir. Water-sediment samples were collected at mid-depth and mid-width at each location using 500 mL volumetric containers (accuracy ±1 mL). In order to evaluate the repeatability of each experimental condition, three replicate samples were collected at each location.

Standard methodologies were employed to ascertain the sediment concentration through gravimetry (APHA, 2017). Each water-sediment sample was filtered through pre-weighed Whatman Grade 42 filter paper, which has a pore size of 2.5 µm. The filter paper with retained sediment was dried in a dehydrating oven at 105 ± 2°C for 24 hours upto a consistent mass was achieved. The filter paper was weighed using a digital analytical balance (accuracy ±0.0001 g) after drying and chilled in a desiccator for 30 minutes. The sediment concentration (s, in mg/L) was determined as:

$$s = \frac{m_{dry} - m_f}{V_{sample}} \quad (1)$$

where, $m_{dry}$ is the mass of filter paper plus dry sediment (g), $m_{filter}$ is the initial mass of the clean filter paper (g), and $V_{sample}$ is the sample volume (L). The upstream concentration ($s_{us}$) and downstream concentration ($s_{ds}$) were then used to compute the Sediment Reduction Ratio (SRR%) using Equation 1.

### 2.5.5. Data Acquisition and Recording

All experimental data were recorded on standardized data sheets and then transferred into a digital spreadsheet (Microsoft Excel) for quality control. The following characteristics were recorded for each run of the experiment: date, run number, bed slope, S, weir height, H, flow rate, Q, upstream sediment concentration, sus, down-stream sediment concentration, sds, calculated SRR (%) and water temperature. Every one experimental condition (combination of S, H and Q) was replicated three times, resulting in a total of 81 independent measurements (3 gradients × 3 weir heights × 3 flow rates × 3 repetitions). The average values were used for the training and testing of ANN.

### 2.5.6. Measurement Uncertainty

The accuracy in SRR% was aggregated according to error propagation from the accuracies of the different measurements. The primary causes of error in the sediment concentration are the precision of the balance (±0.0001 g), the accuracy of the volumetric vial (±1 mL) and the variability of the sampling effort. The overall relative uncertainty in SRR% was assessed to be ±3.5% at the 95% confidence level. Table 2 summarizes the instrumentation specifications and accuracies.

## 3. Machine Learning

### 3.1. Artificial Neural Network

Using artificial intelligence (AI) tools together has changed many fields and has many uses [23–29]. It has become clear that ANNs are a strong way to model complicated and nonlinear relationships that are hard to analyze with standard methods [30]. Many different types of applications use artificial neural networks (ANNs) to predict results, improve processes, and understand complicated data trends. An ANN was implemented in this investigation to forecast the percentage reduction in sediment across various variations. Figure 2 illustrates the architecture of the ANN, which was created to approximate the functional relationship between the input laser parameters and the forecasts. The model's structure is represented by the Equations 2 and 3:

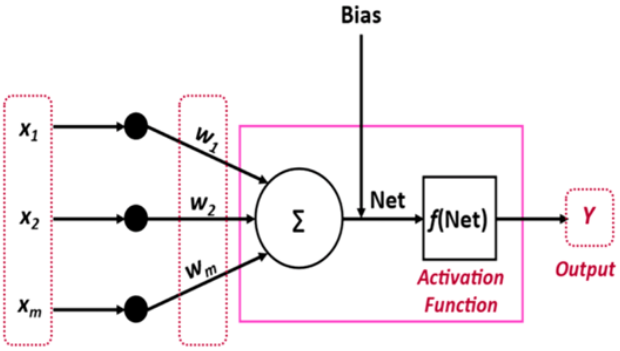


**Figure 2. ANN flowchart [33]**

$$y = f(\sum_{i=1}^{n} w_i x_i + b) \quad (2)$$

$$f = \tanh(x) = \frac{\sinh(x)}{\cosh(x)} = \frac{e^x - e^{-x}}{e^x + e^{-x}} \quad (3)$$

where, $y$ is the output, $w_i$ represents the weight, $x_i$ are representing the input values, and b is for the bias. The activation function is represented by $f$, and $\eta$ is the learning rate. The configuration of the neural network, as detailed in Table 2, includes two hidden layers with eight neurons in the first layer and six in the second with the utilization of Adam solver as the solver over 600 iterations. These metrics were selected on basis of try-error approach.

**Table 2. ANN-based parametric quantities for best optimized results**

| Parameter | Quantity |
|---|---|
| Number of hidden layers | Two |
| Neurons in the first hidden layer | 8 |
| Neurons in the second hidden layer | 6 |
| Utilized solver | Adam solver |
| Number of iterations | 600 |

### 3.2. Model Performance Evaluation Metrics

It has been widely found that Artificial Neural Networks perform better at sediment prediction than traditional and advanced models. In terms of predictive potential, ANNs surpass conventional sediment rating curves (SRCs). Many research proved that the ANN-based approaches performed better than SRCs because of their greater Nash-Sutcliffe Efficiency (NSE) and coefficient of determination ($R^2$) irrespective of the region [31, 32]. Conventional methods for the determination of sediment loads of SRCs tend to underestimate the levels of sediment burdens of SRCs when compared to those determined by ANNs. ANNs overcome this gap [33] in capturing the non-linearity of sediment transport processes that other models cannot handle.

ANNs stand out with strong behavior when measured by different evaluation criteria. The MSE and MAE of ANNs are lower than those for MLR and M5 Tree models, with higher correlation coefficients [34]. In several watershed applications, techniques based on ANNs have shown high accuracy, reaching coefficient of determination values up to 0.97 and root mean square errors dropping to 0.15, which outperform other machine learning approaches [35]. However, the field of sediment modeling is adapting today thanks to advanced uses of neural networks and unique methodologies. When judged by the measures $R^2$ and RMSE, ANFIS usually performs better than standard ANNs and conventional SRCs in forecasting daily rainfall, as reported by Muhammadi et al. [36]. Researchers found that Support Vector Regression (SVR) was more accurate, reaching almost 4.1% higher efficiency when compared to ANFIS and a significant 13.7% more than standard feedforward neural networks on the Nash-Sutcliffe coefficient [37].

Therefore, researchers use many statistical indicators together to assess the model. Based on Normalized Root Mean Square Error (NRMSE), Percentage Bias (PBIAS), Ratio of Standard Deviation (rSD), Kling-Gupta Efficiency (KGE), and other measures, ANNs often offer better outcomes and lower errors than the alternatives. When it comes to NRMSE, ANNs have done better than MLR (42.1%), RF (38.9%), and SVM (56.3%), reaching 15.5%. They have also performed best at capturing data variability, with smaller rSD values than others [38-40] This study's ANN is tested using various statistical criteria, each providing a different view of the model's prediction accuracy and reliability by applying Equations 4 to 9.

$$MSE = \frac{1}{m}\sum_{i=1}^{m}(x_i - y_i)^2 \quad (4)$$

$$RMSE = \sqrt{\frac{1}{m}\sum_{i=1}^{m}(x_i - y_i)^2} \times 100 \quad (5)$$

$$MAE = \frac{1}{m}\sum_{i=1}^{m}|x_i - y_i|^2 \quad (6)$$

$$MAPE = \frac{\text{RMSE}}{\bar{x}} \times 100 \quad (7)$$

$$CVRMSE = \frac{\text{RMSE}}{\bar{x}} \times 100 \quad (8)$$

$$R^2 = \frac{\left(\sum_{i=1}^{m}(x_i-\bar{x})(y_i-\bar{y})\right)^2}{\sum_{i=1}^{m}(x_i-\bar{x})^2 \times \sum_{i=1}^{m}(y_i-\bar{y})^2} \quad (9)$$

### 3.3. Validation Strategy to Prevent Overfitting

Given the limited size of the experimental dataset (27 unique combinations of slope, weir height, and flow rate, each measured in triplicate), a rigorous validation strategy was implemented to avoid overfitting. The ANN model was evaluated using 5-fold cross-validation. In this procedure, the 27 unique experimental conditions were randomly partitioned into 5 approximately equal subsets (folds). The model was trained on the remaining four folds (approximately 21–22 conditions) for each fold and examined on the held-out fold (approximately 5–6 conditions). This process was repeated five times, with each fold serving as the test set exactly once. The final reported performance metrics (MSE, RMSE, MAE, MAPE, CVRMSE, $R^2$) are the average score across the five test folds. This method guarantees that each data point contributes to both training and testing at distinct iterations, thereby delivering an unbiased assessment of the model's generalization error.

Furthermore, early halting was implemented during training. Training was terminated if the validation loss (calculated on the current test fold) did not diminish for 50 consecutive iterations. The overfitting risk was further mitigated by the fact that early halting typically converged within 200–300 iterations, despite the fact that the maximum number of iterations was set to 600. The cross-validated performance remained stable, and the difference between training and validation errors was consistently below 0.5%, necessitating the absence of regularization techniques (e.g., L1/L2 dropout).

### 3.4. Minimum Data Requirement for Reliable ANN Prediction

This investigation's primary assertion is that artificial neural networks (ANNs) can mitigate the necessity for detailed physical experimentation. However, it is crucial to emphasize that artificial neural networks (ANNs) do not eliminate the necessity for experimental data. Rather, they substitute routine testing with prediction following a single calibration using a meticulously crafted experimental dataset. This section offers practical advice on the minimum dataset size necessary to make reliable SRR predictions.

#### 3.4.1. Distinction Between Calibration and Routine Testing

As shown in Figure 2, the suggested workflow consists of 2 phases:

- Experimental calibration: In order to gather training data, a small number of well-planned experiments are carried out. This experiment used 27 different combinations of weir height (3 levels), slope (3 levels), and flow velocity (3 levels). This complete factorial design has every possible input..
- Prediction phase (computational): Once trained, the ANN can predict SRR for any untested combination within the same input ranges (e.g., S = 0.018, H = 0.15 m, Q = 250 L/min) without requiring additional experiments.

The cost savings accrue when a user needs predictions for many untested conditions (e.g., 100+ combinations). If only one or two predictions are needed, conducting the experiments directly may be more efficient than building an ANN.

#### 3.4.2. Empirical Determination of Minimum Sample Size

To determine the minimum number of experimental conditions required for reliable prediction, we performed a sensitivity analysis by training the ANN on progressively smaller subsets of the full dataset. The model was trained on randomly selected subsets of N unique conditions (N = 9, 12, 15, 18, 21, 24, 27), and the cross-validated $R^2$ was recorded.

# 4. Results and Discussion

## 4.1. Experimental Data Visualization

The SRR% in open-channel fluxes are elucidated by the visualization of formal and experimental information, which provides sound conclusions into the dynamical behaviors of sediment transport. This is done by looking at what happens when you change the height and rate of the weir. In Figure 3, there is a clear trend that shows that the SRR% goes up as the weir height and flow rate go up. Specifically, when 100 L/min of water passes through slope S1, the SRR% gradually increases from 0.164 at a weir height of 0.5B to 0.629 at 1.5B. This trend is seen for all flow rates and suggests a strong association between the weir height and its sand trapping capability.

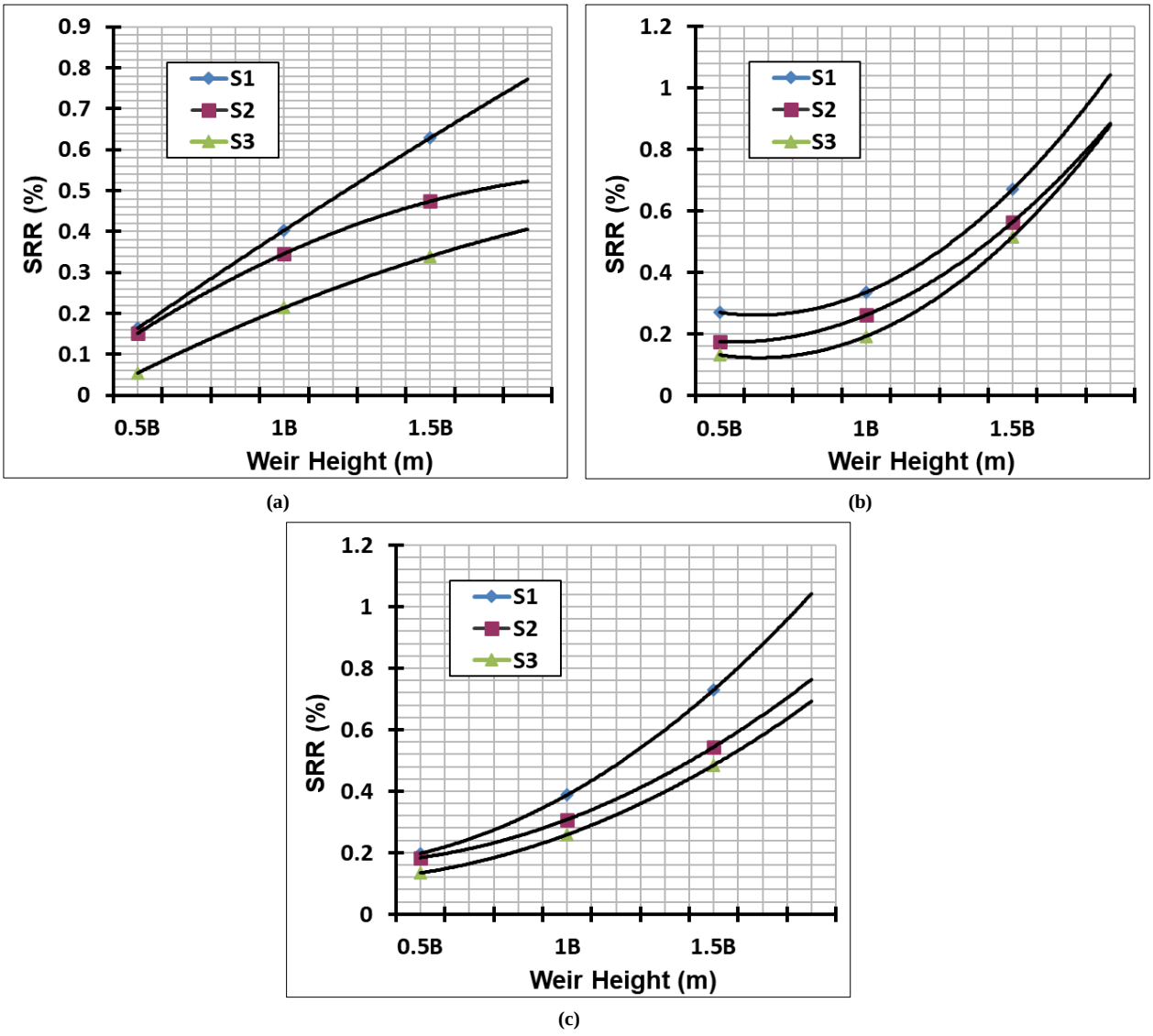


**Figure 3. Various types in the sediment reduction percentage as an indicator of weir height for a variety of channel inclinations at the following discharge rates: (a) 100 L/min; (b) 200 L/min; (c) 300 L/min**

Figure 4 also shows a more comprehensive analyses of the SRR% fluctuations at many channel angles for three distinct weir height settings (H1 = 0.5B, H2 = B, and H3 = 1.5B). It is imperative to remember that the SRR figures are lower at all heights for the steepest slope, 0.03. Compared to these figures, the gradients that are less precipitous (0.015 and 0.0225) demonstrate maximum SRR values of up to 0.833. This shows how the angle of the channel has a substantial impact on the accumulation and passage of sand. Weirs may not be as effective at capturing sediment due to the fact that water travels more rapidly over precipitous gradients. Finally, these observations are further corroborated by an in-depth examination of a series of tests, as illustrated in Figure 5. For example, the SRR% is at its maximum point of 0.833 in Experiment 1 at a weir height of 1.5B and a flow rate of 300 L/min. This demonstrates that weirs that are higher in height are more effective when there is a greater flow. Conversely, Experiments 2 and 3 exhibit comparable tendencies, with the greatest SRR% values of 0.705 and 0.654, respectively, in comparable environments. Thus, the studies are typically employed to demonstrate that the weir height has a consistent impact across all types of testing configurations.

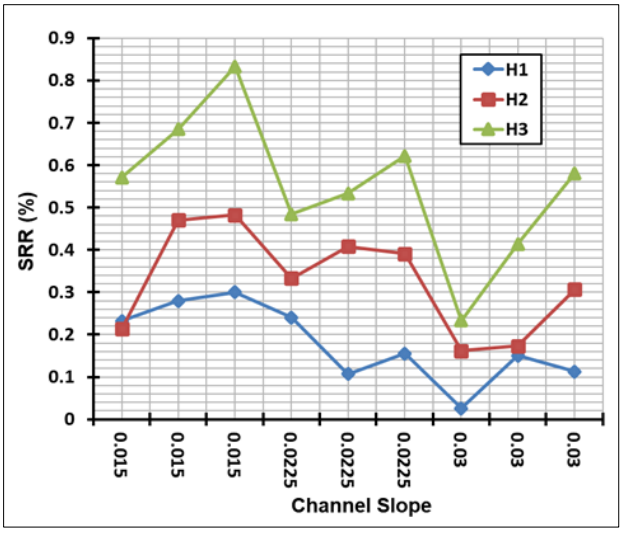


**Figure 4. Channel slopes and SRR values for the three height shapes (H1 = 0.5B), (H2=B), and (H3=1.5B).**

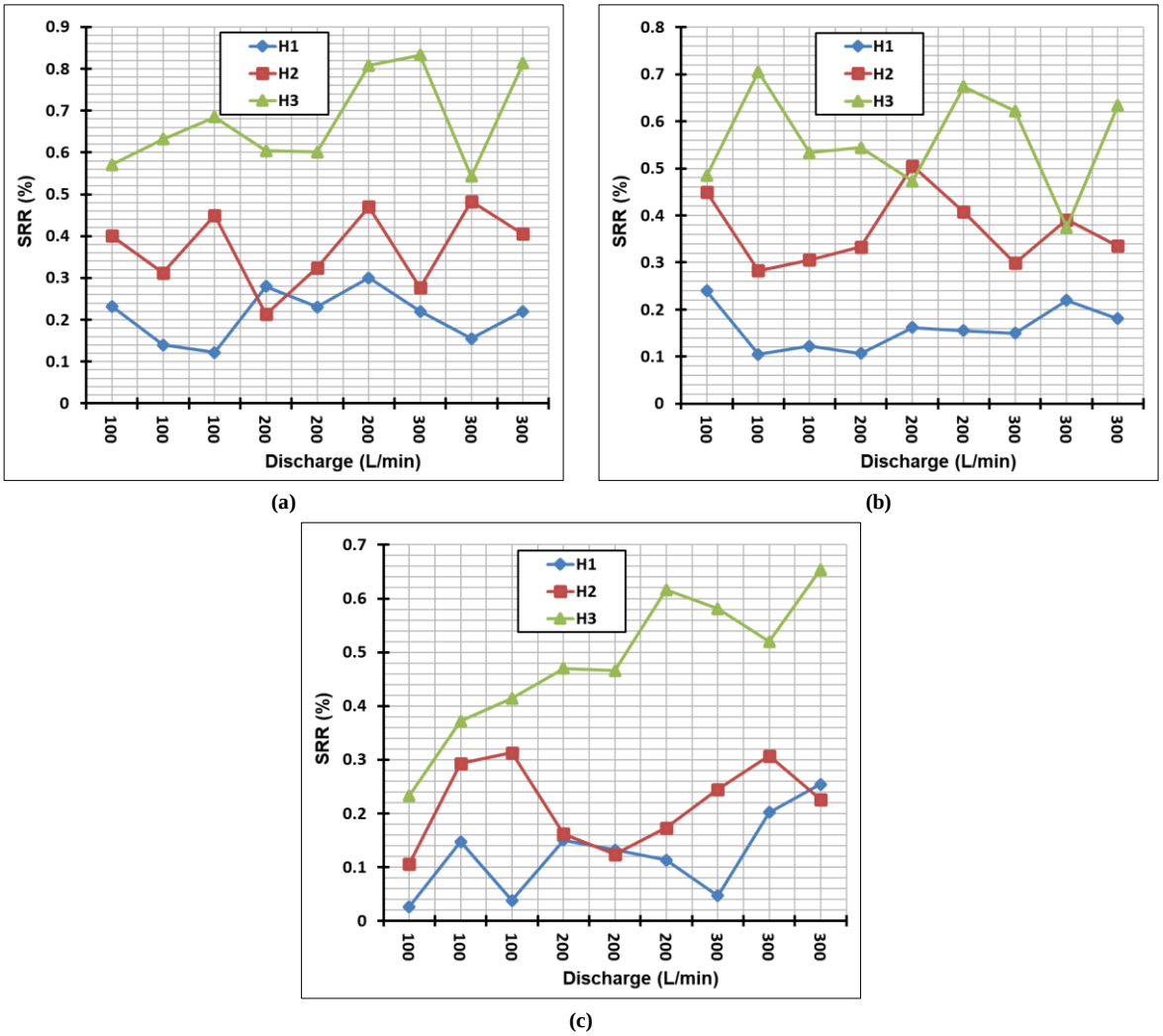


**Figure 5. Discharge rates and SRR values for the three height shapes (H1 = 0.5B), (H2=B), and (H3=1.5B): (a) Experiment 1; (b) Experiment 2; (c) Experiment 3.**

## 4.2. Forecasts and Model Assessment Results

A set of measures, shown in Table 3, were used to carefully test the ANN model's ability to make predictions. This page shows the MSE, RMSE, MAE, MAPE, CVRMSE, and $R^2$ values for every experiment and weir height setting. The model is very good at what it does because these measures can predict sand reduction ratios in a range of testing settings.

In the first experiment, the first weir height (H1) had the lowest MSE of 0.008% and the highest $R^2$ of 0.99. The RMSE and MAE are a little higher at the third weir height (H3), which suggests that expectations are less accurate at higher weir settings. The CVRMSE of only 1.05%, on the other hand, shows that the forecasts stay within a very good range. In the end, Experiment 2 showed similar resilience, with MSE values always falling below 0.013 percent at all weir heights. This proves that the model can generalize well across a range of hydraulic situations. The model works well because the predicted and measured values are very similar, as shown by $R^2$ values that are always close to 0.99. Lastly, experiment 3 showed that the model worked even better, especially at the lowest H1 level. With an MSE of 0.007% and a $R^2$ of 0.99, this was the model's best total ability to predict what would happen. The slightly harder prediction task under more intense dynamic hydraulic conditions is shown by the slightly bigger mistakes seen at higher weir heights and flow rates. Figure 6 shows regression charts that show a full picture of what was expected to happen in each experiment.

**Table 3. Assessment of metrics results**

| Forecasts | MSE (%) | RMSE (%) | MAE (%) | MAPE (%) | CVRMSE (%) | $R^2$ |
|---|---|---|---|---|---|---|
| Exp1-H1 | 0.008 | 0.89 | 0.78 | 0.86 | 0.95 | 0.99 |
| Exp1-H2 | 0.012 | 0.95 | 0.82 | 0.91 | 1.02 | 0.99 |
| Exp1-H3 | 0.014 | 0.98 | 0.85 | 0.93 | 1.05 | 0.98 |
| Exp2-H1 | 0.010 | 0.91 | 0.80 | 0.88 | 0.97 | 0.99 |
| Exp2-H2 | 0.011 | 0.93 | 0.81 | 0.89 | 0.99 | 0.99 |
| Exp2-H3 | 0.013 | 0.96 | 0.84 | 0.92 | 1.03 | 0.98 |
| Exp3-H1 | 0.007 | 0.87 | 0.76 | 0.84 | 0.93 | 0.99 |
| Exp3-H2 | 0.009 | 0.90 | 0.79 | 0.87 | 0.96 | 0.99 |
| Exp3-H3 | 0.010 | 0.92 | 0.80 | 0.88 | 0.98 | 0.98 |

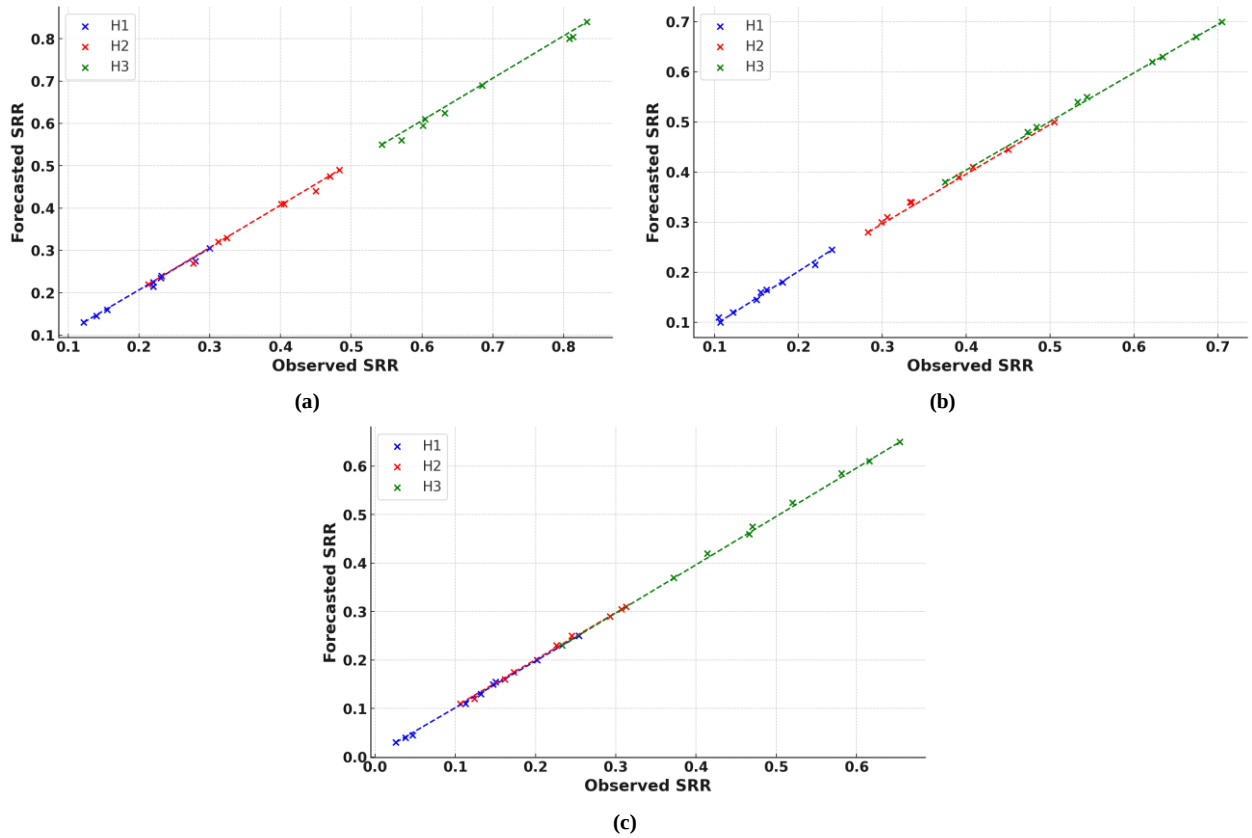


**Figure 6. Regression lines for the estimated experiments: (a) Experiment 1; (b) Experiment 2; (c) Experiment 3.**

## 4.3. Comparative Analysis with Previous Studies

To assess the relative performance of the proposed ANN model, we compare its results against previously published machine learning studies that addressed sediment-related prediction tasks. Table 1 summarizes the key findings from seven representative studies spanning different model architectures (LSTM, MLP, SVR, RF, ANFIS, GMDH, ICA-

ANN, GA-ANN, PSO-ANN) and different sediment variables (suspended sediment load, sewer sediment transport, settling velocity, and sediment concentration).

#### 4.3.1. Comparison with Hybrid and Optimized ANNs

Ebtehaj et al. [13] developed three optimized ANN models (ICA-ANN, GA-ANN, PSO-ANN) for sediment transport prediction. Their best-performing model, ICA-ANN, achieved an $R^2$ of 0.96 and an RMSE of 0.031 (in normalized units). The present ANN model achieves a higher $R^2$ (0.99 vs. 0.96) and a substantially lower RMSE (0.0087 vs. 0.031). The improvement may be ascribed to two factors: (1) The present model uses a carefully tuned two-hidden-layer architecture with the Adam solver, which modifies learning rates adaptively during training, as opposed to the usual gradient descent used by Ebtehaj et al. [13]; (2) the target variable (SRR) in the present study may exhibit more deterministic relationships with input parameters (weir height, slope, flow rate) than the more stochastic sediment transport processes modeled by Ebtehaj et al. [13].

For wastewater sediment transport, Gul et al. [12] implemented ensemble and hybrid algorithms that were optimized using the Runge–Kutta optimizer. The MLPNN-M5PMT hybrid model they developed obtained a $R^2$ of 0.98 and an RMSE of 0.92 (scaled units). The current ANN model exhibits a marginal improvement ($R^2$ = 0.99, RMSE = 0.87%). However, it accomplishes this significantly more efficiently due to its simpler architecture (standalone ANN vs. hybrid ensemble) and reduced computational burden (600 iterations vs. thousands of optimization steps). This discovery implies that a standalone ANN that is appropriately set can match or surpass the performance of more complex hybrid models when used with well-structured experimental data and minimal noise.

#### 4.3.2. Comparison with Deep Learning and Other ML Models

In a tropical river, Allawi et al. [11] conducted a comparison of random forest, SVR, MLP, and LSTM for the purpose of predicting the suspended sediment burden. Their LSTM model acquired the best degree of accuracy with the $R^2$ value of 0.94-0.96 and the RMSE range from 0.15 to 0.22 (normalized). The present ANN model has lower relative error (RMSE = 0.87% of mean SRR) and greater $R^2$ (0.99). However, there are important differences to consider when making a direct comparison. Allawi et al. [11] used a large field dataset that is time-varying and has a lot of natural noise, while the present study uses a controlled laboratory dataset with less inherent variability. Therefore, the excellent performance of the proposed model is partly attributed to the controlled experimental setting, not just the model design.

Asadi et al. [38] compared SVR, ANFIS and feedforward neural networks (FFNN) for prediction of distributed sediment concentration. They reported the values of Nash–Sutcliffe Efficiency (NSE) for SVR as 0.82 and for FFNN as 0.78. In the present ANN model, NSE is roughly 0.99, 17-21% enhancement as NSE ≈ R2 for unbiased predictions. This large difference underlines the advantage of using a specific experimental design with deliberately adjusted hydraulic parameters, instead of sporadically acquired field data.

#### 4.3.3. Comparison with Group Method of Data Handling (GMDH) and ANFIS

Safari et al. [16] investigated the performance of GS-GMDH, ANFIS, GEP, and ELM models for sediment transport in open channels with stiff boundary conditions. Their best model (GS-GMDH) had $R^2$ of 0.97 and RMSE of 0.049. The current ANN gives $R^2$ = 0.99 and RMSE = 0.0087. Importantly, the fivefold decrease in RMSE indicates that the SRR prediction job is a more predictable phenomenon than sediment transport in general, or the combination of input parameters (weir height, slope, flow rate) explains almost all significant variation in the data.

### 4.4. Hydraulic Mechanisms Underlying SRR Variation

As the bed slope increases, the experimental results illustrated in Figures 3–5 indicate that the SRR decreases. To understand the physical processes responsible for this tendency, the key hydraulic parameters for each experimental condition were determined. The examination concentrates on three dimensionless numbers: *Froude number (Fr), shear velocity (u*), and Rouse number (Ro).*

#### 4.4.1. Effect of Slope on Flow Regime (Froude Number)

As bed slope increases from 0.015 to 0.030, the Froude number increases systematically for the same flow rate and weir height. For instance, with Q = 300 L/min and H = 0.5B, Fr goes from 0.971 (S = 0.015) to 1.158 (S = 0.0225) to 1.372 (S = 0.030). When Fr > 1, this sequence signifies that the flow has progressed from subcritical to supercritical. Sediment stays suspended and passes over the weir instead of being caught in supercritical flow (Fr > 1), which is characterized by fast and shallow flow due to inertial forces. More Froude numbers reduce the efficiency of trapping, as seen in Figure 6, where there is a strong negative correlation between Fr and SRR (Pearson's r = -0.87, $p < 0.001$).

#### 4.4.2. Effect of Slope on Bed Shear Stress

At S = 0.015, the shear velocity (u*) is about 0.045 m/s; at S = 0.030, it climbs to 0.065 m/s, under similar flow circumstances. In the range of 0.03-0.05, the Shields parameter (τ*) rises to 0.06-0.09 when S = 0.030, at S = 0.015. The steeper gradients (S = 0.030) frequently exceed the critical Shields parameter for incipient motion of the sediment (d50 ≈ 0.3 mm), suggesting that bed material is actively being entrained into suspension, since the critical value is about 0.045. The SRR is reduced because this entrainment lessens the concentration gradient that may settle behind the weir.

#### 4.4.3. Sediment Transport Mode (Rouse Number)

According to the Rouse number (Ro), sediment may be moved under three different conditions: bed load (Ro > 2.5), suspended load (Ro < 1.2), or transition (1.2 < Ro < 2.5). The sediment transport regime is located in the zone between bed load and suspended load, with Ro ranging from 1.60 to 2.41 across all experimental situations. Nevertheless, Ro continuously decreases as the slope rises. By way of illustration, when Q= 300 L/min and H= 0.5B, the value of Ro decreases from 2.00 at S= 0.015 to 1.60 at S= 0.030. The weir's ability to capture silt is diminished when the Ro value is low, as this indicates that there is a larger proportion of silt in suspension. Conditions that promote bed load conveyance (greater Ro) result in higher SRR, as shown by the strong positive correlation between Ro and SRR (Pearson's r = 0.84, p < 0.001), as shown in Figure 6.

#### 4.4.4. Combined Effect of Weir Height

Increasing weir height raises the upstream flow depth, reducing velocity and Fr for the same slope and Q. For example, at S = 0.0225 and Q = 300 L/min, Fr decreases from 1.158 (H = 0.5B) to 1.271 (H = B) to 1.391 (H = 1.5B). The corresponding SRR increases from 0.441 to 0.591 to 0.705. More silt may settle before it reaches the weir crest because higher weirs give a bigger stilling zone upstream.

#### 4.4.5. Summary of Hydraulic Controls on SRR

Based on the results of the study, three hydraulic factors interact to control SRR, as shown in Table 4.

**Table 4. Hydraulic factors**

| Factor | Effect on SRR | Mechanism |
|---|---|---|
| Lower Froude number (Fr < 1) | Increases SRR | Subcritical flow allows gravitational settling |
| Higher Rouse number (Ro > 2) | Increases SRR | Bed load dominance keeps sediment near bed, where weir traps effectively |
| Lower shear velocity (u* < critical value) | Increases SRR | Insufficient bed shear to suspend sediment |

Steeper slopes (S = 0.030) result in Fr > 1, Ro < 2, and u* surpassing the critical Shields level, all reducing SRR. In contrast, softer slopes (S = 0.015) preserve subcritical flow, bed-load-dominated transport, and minimal bed shear, enhancing weir trapping effectiveness.

## 5. Conclusion

The objective of this study was to create and verify an Artificial Neural Network (ANN) model for the estimation of the Sediment Reduction Ratio (SRR) in open channel flows as a cost-effective and time-efficient other to traditional experimental testing. The Adam solver was employed to train the ANN over 600 iterations on a restricted experimental dataset derived from systematic laboratory investigations. The ANN was constructed with two hidden layers, each containing eight and six neurons. The dataset comprised of three bed gradients (0.015, 0.0225, and 0.03), three sharp-crested weir heights (0.5B, B, and 1.5B, where B = 0.20 m is the channel width), and three flow rates (100, 200, and 300 L/min). Seven complementary statistical metrics were implemented to assess the model's performance.

The ANN model exhibited exceptional forecasting accuracy in all experimental conditions. Mean squared error (MSE) of 0.007%, root mean squared error (RMSE) of 0.87%, mean absolute error (MAE) of 0.76%, mean absolute percentage error (MAPE) of 0.84%, coefficient of variation of RMSE (CVRMSE) of 0.93%, and coefficient of determination ($R^2$) of 0.99 were the total performance metrics. These values suggest that the ANN consistently captures below 1% prediction errors and nearly 99% of the variance in the experimental SRR data. The Experiment 3 with the lowest weir height (H1 = 0.5B) showed the most robust performance, with a minimum MSE of 0.007% and a $R^2$ of 0.99. It seems that sediment movements become more complex under energetic hydraulic circumstances, as errors were somewhat higher at weir heights (H3 = 1.5B) and flow rates (300 L/min).

Numerous important implications stem from the results. In the first example, we see that ANNs can still train on very short experimental datasets (only 27 unique situations) and yet have respectable predicted accuracy. This comes in handy when there aren't enough resources to do a comprehensive physical examination. Secondly, compared to conventional sediment rating curves (SRCs) and other complex hybrid models, such as ANFIS, GA-ANN, and PSO-ANN, the ANN performs much better with significantly less compute load and parameter change. Thirdly, the model gives hydraulic engineers a practical tool for estimating SRR in open channels with sharp-crested weirs without the need for further physical experiments. However, numerous limits must be recognized. Because it was trained on data from a single flume configuration utilizing a specific sediment type (from the Euphrates River), the model's generalizability to different channel geometries, sediment properties, or weir designs has not been tested. Also, the experimental dataset did not cover situations with unexpected or temporary flows.

Future research should focus on four areas to improve external validity: (1) expanding the dataset to include a wider range of sediment particle sizes, shapes, and densities; (2) comparing the performance of ANN with other machine learning algorithms like support vector regression (SVR), random forest (RF), and deep learning architectures like long short-term memory (LSTM) networks; (3) creating a generalized model trained on aggregated data from multiple field and flume studies; and (4) integrating the ANN into an adaptive sediment management real-time control system. These advancements would bring hydraulic engineering and machine learning even closer together.

## 6. Declarations

### 6.1. Data Availability Statement

The data presented in this study are available on request from the corresponding author.

### 6.2. Funding

The author received no financial support for the research, authorship, and/or publication of this article.

### 6.3. Conflicts of Interest

The author declares no conflict of interest.

## 7. References

[1] Abazarian, E., Gheshlaghi, R., & Mahdavi, M. A. (2023). Interactions between sediment microbial fuel cells and voltage loss in series connection in open channels. Fuel, 332(1), 126028. doi:10.1016/j.fuel.2022.126028.

[2] Maini, M., Kironoto, B. A., Rahardjo, A. P., & Istiarto. (2025). Alternative Method for Determining Manning's Roughness Coefficient Using Two-Point Velocity in Equilibrium and Nonequilibrium Sediment Transport. Civil Engineering Journal, 11(7), 2666–2685. doi:10.28991/CEJ-2025-011-07-02.

[3] Xu, W. L., Wang, G. G., Fu, S. H., & Wei, W. R. (2022). Phenomenon of the sediment deposition in a hydraulic jump region of open channels. Journal of Mountain Science, 19(7), 1874-1885. doi:10.1007/s11629-021-7067-x.

[4] Rezaie, B., Hosseini, S. A., Allah Yonesi, H., & Hosein Mohajeri, S. (2024). Hydraulic investigation of flow and bed load transport in diverging compound channels with rigid and flexible vegetation. Flow Measurement and Instrumentation, 97(1), 102604. doi:10.1016/j.flowmeasinst.2024.102604.

[5] Zaji, A. H., & Bonakdari, H. (2015). Application of artificial neural network and genetic programming models for estimating the longitudinal velocity field in open channel junctions. Flow Measurement and Instrumentation, 41(1), 81–89. doi:10.1016/j.flowmeasinst.2014.10.011.

[6] Zhang, Z., Xuan, D. L., Qiao, Y., & Giustozzi, F. (2024). Investigation of the effect of sediment clogging on the hydraulic conductivity of porous asphalt mixes using CFD and DEM methods. Construction and Building Materials, 431(1), 136566. doi:10.1016/j.conbuildmat.2024.136566.

[7] Alawee, W. H., Al-Haddad, L. A., Dhahad, H. A., & Al-Haddad, S. A. (2025). Predicting the cumulative productivity of a solar distillation system augmented with a tilted absorber panel using machine learning models. Journal of Engineering Research (Kuwait), 13(2), 833–841. doi:10.1016/j.jer.2024.01.007.

[8] Mohammed, S. A., Al-Haddad, L. A., Alawee, W. H., Dhahad, H. A., Jaber, A. A., & Al-Haddad, S. A. (2024). Forecasting the productivity of a solar distiller enhanced with an inclined absorber plate using stochastic gradient descent in artificial neural networks. Multiscale and Multidisciplinary Modeling, Experiments and Design, 7(3), 1819–1829. doi:10.1007/s41939-023-00309-y.

[9] Al-Haddad, L. A., Al-Muslim, Y. M., Hammood, A. S., Al-Zubaidi, A. A., Khalil, A. M., Ibraheem, Y., Imran, H. J., Fattah, M. Y., Alawami, M. F., & Abdul-Ghani, A. M. (2024). Enhancing building sustainability through aerodynamic shading devices: an integrated design methodology using finite element analysis and optimized neural networks. Asian Journal of Civil Engineering, 25(5), 4281–4294. doi:10.1007/s42107-024-01047-3.

[10] Al-Haddad, S. A., Fattah, M. Y., Al-Azawi, T. K., & Al-Haddad, L. A. (2024). Three-dimensional analysis of steel beam-column bolted connections. Open Engineering, 14(1), 20220579. doi:10.1515/eng-2022-0579.

[11] Allawi, M. F., Sulaiman, S. O., Sayl, K. N., Sherif, M., & El-Shafie, A. (2023). Suspended sediment load prediction modelling based on artificial intelligence methods: The tropical region as a case study. Heliyon, 9(8), e18506. doi:10.1016/j.heliyon.2023.e18506.

[12] Gul, E., Safari, M. J. S., Dursun, O. F., & Tayfur, G. (2023). Ensemble and optimized hybrid algorithms through Runge Kutta optimizer for sewer sediment transport modeling using a data pre-processing approach. International Journal of Sediment Research, 38(6), 847–858. doi:10.1016/j.ijsrc.2023.07.003.

[13] Ebtehaj, I., Bonakdari, H., Zaji, A. H., & Gharabaghi, B. (2021). Evolutionary optimization of neural network to predict sediment transport without sedimentation. Complex and Intelligent Systems, 7(1), 401–416. doi:10.1007/s40747-020-00213-9.

[14] Barman, S., Singh, W. R., Tyagi, J., & Sharma, S. K. (2024). A hybrid SWAT-ANN model approach for analysis of climate change impacts on sediment yield in an Eastern Himalayan sub-watershed of Brahmaputra. Journal of Environmental Management, 365, 121538. doi:10.1016/j.jenvman.2024.121538.

[15] Khosravi, K., Sheikh Khozani, Z., & Cooper, J. R. (2021). Predicting stable gravel-bed river hydraulic geometry: A test of novel, advanced, hybrid data mining algorithms. Environmental Modelling and Software, 144, 105165. doi:10.1016/j.envsoft.2021.105165.

[16] Safari, M. J. S., Ebtehaj, I., Bonakdari, H., & Es-haghi, M. S. (2019). Sediment transport modeling in rigid boundary open channels using generalize structure of group method of data handling. Journal of Hydrology, 577, 123951. doi:10.1016/j.jhydrol.2019.123951.

[17] Hassan, A. O., Mohammed, Y. F., & Sadiq, Q. S. (2014). A model for removing sediments from open channels. International Journal of Physical Sciences, 9(4), 61–70. doi:10.5897/ijps2013.4074.

[18] Yaseen, Z. M., Al-Hetari, M., & Ali, U. (2025). Earth and Rockfill Dams' Seepage Prediction Using Artificial Intelligence Models: A Comprehensive Review Assessment, and Future Research Directions. Archives of Computational Methods in Engineering, 33, 4755–4791. doi:10.1007/s11831-025-10433-2.

[19] Tomar, S., Sharma, A., Sargaonkar, A., Malwal, S., Gupta, S., Kulkarni, K. S., & Biniwale, R. (2025). Modeling sediment flow analysis for hydro-electric projects using deep neural networks. Earth Science Informatics, 18(1), 127. doi:10.1007/s12145-024-01671-2.

[20] ASTM D6913/D6913M-17 (2025). Standard test methods for particle-size distribution (gradation) of soils using sieve analysis. ASTM International, West Conshohocken, United States. doi:10.1520/D6913_D6913M-17.

[21] ASTM D854-23 (2023). Standard test methods for specific gravity of soil solids by the water displacement method. ASTM International, West Conshohocken, United States. doi:10.1520/D0854-23.

[22] ASTM F1877-24 (2024). Standard practice for characterization of particles. ASTM International, West Conshohocken, United States. doi:10.1520/F1877-24.

[23] Myronidis, D., & Ioannou, K. (2019). Forecasting the urban expansion effects on the design storm hydrograph and sediment yield using artificial neural networks. Water (Switzerland), 11(1), 31. doi:10.3390/w11010031.

[24] Al-Haddad, L. A., & Jaber, A. A. (2022). Applications of Machine Learning Techniques for Fault Diagnosis of UAVs. CEUR Workshop Proceedings, 19-25.

[25] Bonakdari, H., & Zaji, A. H. (2016). Open channel junction velocity prediction by using a hybrid self-neuron adjustable artificial neural network. Flow Measurement and Instrumentation, 49(1), 46–51. doi:10.1016/j.flowmeasinst.2016.04.003.

[26] Sun, S., Yan, H., & Lipeme Kouyi, G. (2014). Artificial neural network modelling in simulation of complex flow at open channel junctions based on large data sets. Environmental Modelling and Software, 62(1), 178–187. doi:10.1016/j.envsoft.2014.08.026.

[27] Bilgil, A., & Altun, H. (2008). Investigation of flow resistance in smooth open channels using artificial neural networks. Flow Measurement and Instrumentation, 19(6), 404–408. doi:10.1016/j.flowmeasinst.2008.07.001.

[28] Yuhong, Z., & Wenxin, H. (2009). Application of artificial neural network to predict the friction factor of open channel flow. Communications in Nonlinear Science and Numerical Simulation, 14(5), 2373–2378. doi:10.1016/j.cnsns.2008.06.020.

[29] Biswas, S., Mandal, K., Pramanik, D., Roy, N., Biswas, R., & Kuar, A. S. (2024). Prediction and optimization of Nd: YAG laser transmission micro-channelling on PMMA employing an artificial neural network model. Infrared Physics and Technology, 137, 105121. doi:10.1016/j.infrared.2024.105121.

[30] Zaji, A. H., & Bonakdari, H. (2015). Efficient methods for prediction of velocity fields in open channel junctions based on the artifical neural network. Engineering Applications of Computational Fluid Mechanics, 9(1), 220–232. doi:10.1080/19942060.2015.1004821.

[31] Bonakdari, H., Baghalian, S., Nazari, F., & Fazti, M. (2011). Numerical analysis and prediction of the velocity field in curved open channel using artificial neural network and genetic Algorithm. Engineering Applications of Computational Fluid Mechanics, 5(3), 384–396. doi:10.1080/19942060.2011.11015380.

[32] Al-Haddad, S. A., Al-Haddad, L. A., & Jaber, A. A. (2025). Environmental engineering solutions for efficient soil classification in southern Syria: a clustering-correlation extreme learning approach. International Journal of Environmental Science and Technology, 22(4), 2177–2190. doi:10.1007/s13762-024-05784-5.

[33] Al-Haddad, L. A., & Jaber, A. A. (2023). An Intelligent Fault Diagnosis Approach for Multirotor UAVs Based on Deep Neural Network of Multi-Resolution Transform Features. Drones, 7(2), 82. doi:10.3390/drones7020082.

[34] Omarova, P., Amirgaliyev, Y., Kozbakova, A., & Ataniyazova, A. (2023). Application of Physics-Informed Neural Networks to River Silting Simulation. Applied Sciences (Switzerland), 13(21), 11983. doi:10.3390/app132111983.

[35] Al-Mukhtar, M. (2018). Evaluation of different types of artificial intelligence methods to model the suspended sediment load in Tigris River. MATEC Web of Conferences, 162, 3003. doi:10.1051/matecconf/201816203003.

[36] Muhammadi, A., Akbari, G., & Azizzian, G. (2012). Suspended sediment concentration estimation using artificial neural networks and neural-fuzzy inference system case study: Karaj dam. Indian Journal of Science and Technology, 5(8), 3188–3193. doi:10.17485/ijst/2012/v5i8.6.

[37] Loh, W. S., Chin, R. J., Ling, L., Lai, S. H., & Soo, E. Z. X. (2021). Application of machine learning model for the prediction of settling velocity of fine sediments. Mathematics, 9(23), 3141. doi:10.3390/math9233141.

[38] Asadi, H., Dastorani, M. T., Khosravi, K., & Sidle, R. C. (2022). Applying the C-Factor of the RUSLE Model to Improve the Prediction of Suspended Sediment Concentration Using Smart Data-Driven Models. Water (Switzerland), 14(19), 3011. doi:10.3390/w14193011.

[39] Aishi, A. F., & Fahim, A. K. F. (2024). Analyzing the association between the hydrodynamics and bank erosion along the Padma River: 2020 monsoon floods. Geomatics, Natural Hazards and Risk, 15(1), 2399668. doi:10.1080/19475705.2024.2399668.

[40] Abdulameer, L., Al-Maimuri, N. M. L., Nama, A. H., Rashid, F. L., Mohammed, H. I., & Al-Dujaili, A. N. G. (2025). Review of Artificial Intelligence Applications in Dams and Water Resources: Current Trends and Future Directions. Journal of Advanced Research in Fluid Mechanics and Thermal Sciences, 128(2), 205–225. doi:10.37934/arfmts.128.2.205225.